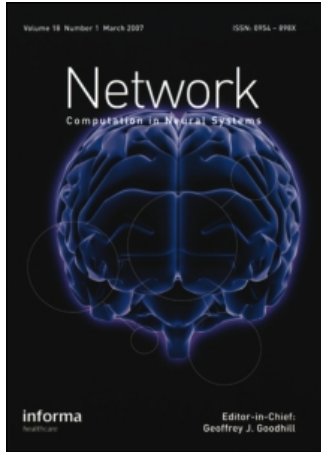


This article was downloaded by:[Max Planck Inst & Research Groups Consortium]
On: 4 September 2007
Access Details: [subscription number 771335669]
Publisher: Informa Healthcare
Informa Ltd Registered in England and Wales Registered Number: 1072954
Registered office: Mortimer House, 37-41 Mortimer Street, London W1T 3JH, UK



Network: Computation in Neural Systems

Publication details, including instructions for authors and subscription information:
<http://www.informaworld.com/smpp/title~content=t713663148>

Analysis of ocular dominance pattern formation in a high-dimensional self-organizing-map model

H-U Bauer^{ab}; D. Brockmann^a; T. Geisel^{ab}

^a Max-Planck-Institut für Strömungsforschung, Göttingen, Germany

^b Sonderforschungsbereich Nichtlineare Dynamik, Universität Frankfurt, Frankfurt/Main, Germany

Online Publication Date: 01 February 1997

To cite this Article: Bauer, H-U, Brockmann, D. and Geisel, T. (1997) 'Analysis of ocular dominance pattern formation in a high-dimensional self-organizing-map model', Network: Computation in Neural Systems, 8:1, 17 - 33

To link to this article: DOI: 10.1088/0954-898X/8/1/004

URL: <http://dx.doi.org/10.1088/0954-898X/8/1/004>

PLEASE SCROLL DOWN FOR ARTICLE

Full terms and conditions of use: <http://www.informaworld.com/terms-and-conditions-of-access.pdf>

This article maybe used for research, teaching and private study purposes. Any substantial or systematic reproduction, re-distribution, re-selling, loan or sub-licensing, systematic supply or distribution in any form to anyone is expressly forbidden.

The publisher does not give any warranty express or implied or make any representation that the contents will be complete or accurate or up to date. The accuracy of any instructions, formulae and drug doses should be independently verified with primary sources. The publisher shall not be liable for any loss, actions, claims, proceedings, demand or costs or damages whatsoever or howsoever caused arising directly or indirectly in connection with or arising out of the use of this material.

© Taylor and Francis 2007

Analysis of ocular dominance pattern formation in a high-dimensional self-organizing-map model

H-U Bauer^{†‡§}, D Brockmann[†] and T Geisel^{†‡}

[†] Max-Planck-Institut für Strömungsforschung, Postfach 2853, 37018 Göttingen, Germany

[‡] Sonderforschungsbereich Nichtlineare Dynamik, Universität Frankfurt, Robert-Mayer-Strasse 8-10, 60054 Frankfurt/Main, Germany

Received 9 September 1996

Abstract. Using a distortion measure for the states emerging in self-organizing maps (SOMs) we mathematically analyse a recently proposed high-dimensional map formation model for ocular dominance patterns. We calculate critical values of parameters for ocular dominance states to occur, and we determine how the pattern layout depends on these parameters. The analysis reveals an increase of ocular dominance bandwidth with decreasing correlation, consistent with a recently observed increase of bandwidth in strabismic cats. In subsequent simulations these analytical results are corroborated, irrespective of the specific normalization procedure (multiplicative or subtractive) employed in the simulations.

1. Introduction

The activity-driven self-organization of neural maps has been described by numerous map formation models. A non-exhaustive list includes: the models of von der Malsburg (1973), Willshaw and von der Malsburg (1976) and Swindale (1980); the correlation-based models of Miller *et al* (1989) and Miller (1994); the elastic net models of Durbin and Mitchison (1990) and Goodhill and Willshaw (1990); Tanaka's model (Tanaka 1990); and models based on Kohonen's self-organizing map (SOM) algorithm (Obermayer *et al* 1990, 1992, Goodhill 1993, Bauer 1995). For recent reviews, see Erwin *et al* (1995) and Swindale (1996). In these models different types of neural map formation, like the development of ocular dominance columns or the development of orientation columns, can be investigated by changing the projection geometry and parametrization, while keeping the general mathematical framework intact.

Using numerical simulations, one can demonstrate that a model can bring about a specific map formation phenomenon at a specific set of parameters. Other types of questions (such as how patterns depend on parameters, or whether a particular behaviour of a model can be ruled out) require systematic variations of parameters, which are numerically costly and cumbersome at best, and infeasible at worst. Here, a mathematical analysis of the pattern formation behaviour is advantageous. It allows us to separate important from unimportant parameters and to calculate regimes in parameter space where a particular type of pattern (a state) of the map can be expected to result from the map formation process. nevertheless, a mathematical analysis is often difficult due to the nonlinearities inherent to many map formation models.

§ E-mail: bauer@chaos.uni-frankfurt.de

Recently, a new analysis technique has been introduced for the high-dimensional version of the SOM algorithm (Bauer *et al* 1996, Riesenhuber *et al* 1997a). It is based on a comparison of energy values for different final map states. While generally it is difficult to assume a final map state in terms of receptive field profiles, the new method takes advantage of the highly nonlinear winner-take-all rule of the SOM and characterizes map states in terms of the ways stimuli are projected to the map. Since this method does not exploit linear instabilities occurring in the map formation dynamics, but focuses on the final map state, it includes the effects of pattern rearrangement during the nonlinear phase of the formation dynamics.

In the present paper we use this technique to analyse an SOM-based model for the development of monocular receptive fields and the ocular dominance map layout. The model is very close to the model introduced and numerically investigated by Goodhill (1993). It deviates from Goodhill's formulation in the choice of stimuli and a technical aspect of the normalization employed in the learning rule (multiplicative versus subtractive normalization, see section 4.3). After a brief sketch of the ocular dominance model and of general aspects of the analysis technique in the second and third section, we describe the actual mathematical analysis and its results in the fourth section. The assumptions made to obtain sensible final states of the map are also detailed in the fourth section. In the fifth section we describe results of simulations, which not only corroborate our analytical results, but which allow us to compare the impact of multiplicative versus subtractive normalization in this model. A brief discussion concludes the paper.

2. SOM model for the development of ocular dominance bands

2.1. The SOM rule

A self-organizing map (Kohonen 1982) is a projection rule for stimuli v in an input space \mathcal{V} to neurons r in an output space \mathcal{C} , together with a dynamics rule specifying the learning of this projection. The SOM is formally described by receptive field vectors $w_r \in \mathcal{V}$ belonging to the nodes r . The projection rule holds that a stimulus is mapped to that map neuron s the receptive field vector of which has the largest overlap with v ,

$$v \mapsto s : w_s \cdot v = \max_r (w_r \cdot v).$$

By this strongly nonlinear mapping rule, the stimulus space \mathcal{V} is tessellated in disjoint regions

$$\Omega_r = \{v \in \mathcal{V} \mid w_r \cdot v > w_{r'} \cdot v \quad \forall \quad r' \neq r\}.$$

Ω_r is called a Voronoi polygon or tessellation region. It contains all stimuli $v \in \Omega_r$ that are mapped to neuron r .

In the SOM, the receptive field vectors w_r are adapted by successive application of stimuli randomly chosen from a probability distribution $P(v)$. The receptive field vectors are incremented as follows:

$$\Delta w_r = \epsilon h(r - s)(v - w_r) \quad (1)$$

with

$$h(r - s) = \exp\left(-\frac{(r - s)^2}{2\sigma^2}\right). \quad (2)$$

The Gaussian $h(r - s)$ occurring in equation (2) is a function of the distance between cortical response unit r and the winning unit s . It is assumed to capture the consequences of the

lateral cortical interactions (for a discussion of the physiological interpretation of the SOM rule, see Kohonen (1995)). The width parameter σ of the Gaussian is a central parameter of the SOM, governing the occurrence or non-occurrence of patterns in the map. The scalar ϵ controls the magnitude of increments. For a more detailed description of the SOM rule, and its applications in biological modelling and technical signal processing, the reader is referred to Kohonen (1995) and Ritter *et al* (1992).

2.2. Architecture of the ocular dominance model

Similarly to the model of Goodhill (1993), two retinal input layers map onto a cortical response layer, see figure 1. Each layer, retinal as well as cortical, consists of $N \times N$ nodes. Nodes in the cortical layer are two-dimensional discrete vectors denoted by $\mathbf{r} = (r_1, r_2)^t$, whereas nodes in the retinal input layers are denoted by $\mathbf{x} = (x_1, x_2)^t$. Deviating from Goodhill's model, we here choose a stimulus to consist of Gaussian activity distributions in both input layers, with relative height 1 in one retina, and height $c \in [0, 1]$ in the other retina. The parameter c controls the degree of correlation between left eye and right eye inputs. Both Gaussians have their centre at \mathbf{x}_0 and have a width σ_s . Formally, a stimulus has two components $\mathbf{v} = (v^l, v^r)^t$, the first component describing the activity distribution in the left, the second in the right input layer. Thus, a right eye (left eye) bias stimulus is (including a normalizing constant α) given by

$$\begin{aligned} \text{right eye bias: } v^{x_0, l}(\mathbf{x}) &= \alpha \exp\left(-\frac{(\mathbf{x} - \mathbf{x}_0)^2}{2\sigma_s^2}\right) \cdot (1, c)^t \\ \text{left eye bias: } v^{x_0, r}(\mathbf{x}) &= \alpha \exp\left(-\frac{(\mathbf{x} - \mathbf{x}_0)^2}{2\sigma_s^2}\right) \cdot (c, 1)^t. \end{aligned}$$

Dominance of the left eye or the right eye input are chosen at random, as well as the centre positions \mathbf{x}_0 .

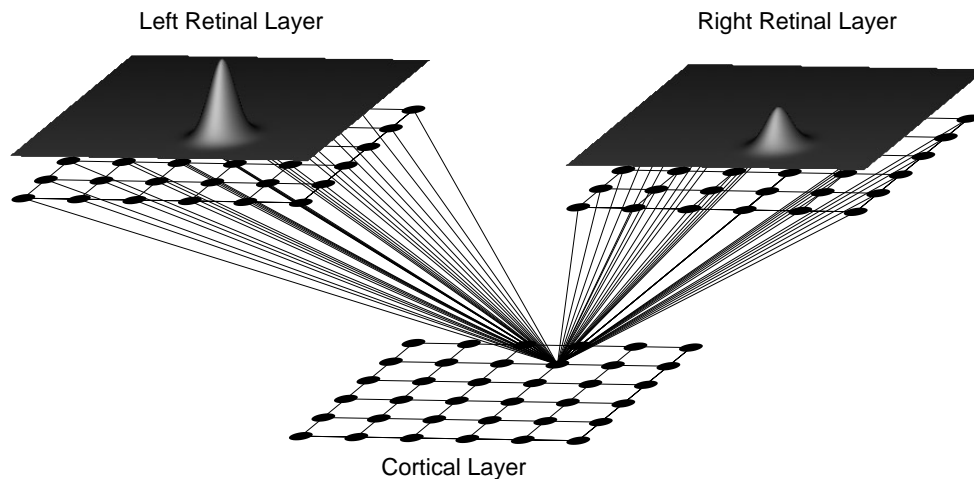


Figure 1. The model architecture. Two retinal input layers are mapped onto a single cortical output layer. Each output unit r receives inputs from each input unit of both layers by synaptic weights w_r . The stimuli are Gaussian activity distributions peaked at the same location in both input layers, one of them attenuated by a factor c .

Since each of the two input layers has as many channels (with locations \mathbf{x}_0) as there are cortical nodes, \mathbf{v} and \mathbf{w}_r are characterized by $2N^2$ values. The stimuli are normalized such that they represent an activity distribution, i.e. such that the sum over these $2N^2$ values has

$$\sum_{\mathbf{x}} v_l(\mathbf{x}) + v_r(\mathbf{x}) = 1. \quad (3)$$

The normalization (3) of the stimuli is automatically imposed also on the receptive field vectors \mathbf{w}_r by the learning rule (1), see Ritter *et al* (1992).

3. Mathematical criteria for the emergence of ocular dominance patterns

3.1. Distortion measure for SOMs

A mathematical analysis of SOMs can be based on a consideration of energy functions, and the lowest energy state. Even though it is known that no exact energy function of the SOM exists (Erwin *et al* 1992), the approximative energy function

$$E_w = \sum_{\mathbf{r}, \mathbf{r}'} \sum_{\mathbf{v} \in \Omega_{\mathbf{r}}} h(\mathbf{r} - \mathbf{r}') (\mathbf{v} - \mathbf{w}_r)^2 \quad (4)$$

could be considered instead (see Kohonen (1995) for a general discussion of energy functions in SOMs, and Mitchison (1995) for a comparison of different approximative energy functions). In the sum over all \mathbf{r}, \mathbf{r}' , the contributions with $\mathbf{r} = \mathbf{r}'$ correspond to the mean square error of a regular vector quantizer. The further contributions with $\mathbf{r} \neq \mathbf{r}'$ include the effect of topography in the map and punish large distances between receptive fields of closeby neurons. However, the usefulness of E_w for an analysis of high-dimensional SOMs is severely restricted by the necessity to know (or make an ansatz for) the receptive field vectors \mathbf{w}_r . For high-dimensional SOMs there is no way known to obtain the \mathbf{w}_r apart from actually simulating the map.

Recently, a further approximation to equation (4) has been proposed (Bauer *et al* 1996), leading to a ‘distortion measure’

$$E_v = \sum_{\mathbf{r}, \mathbf{r}'} \sum_{\mathbf{v} \in \Omega_{\mathbf{r}}, \mathbf{v}' \in \Omega_{\mathbf{r}'}} h(\mathbf{r} - \mathbf{r}') (\mathbf{v} - \mathbf{v}')^2. \quad (5)$$

Expressing the receptive field shapes \mathbf{w}_r as a suitable superposition of stimuli, expanding equations (4) and (5) and comparing terms shows that E_v is related to E_w predominantly by a multiplicative factor (balancing the additional sum in (5), for a more detailed discussion see Riesenhuber *et al* (1997a)). So we can assume that E_v attains a minimum at approximately the same value of \mathbf{w}_r which minimizes E_w .

The main advantage of E_v over E_w lies in the fact that for an evaluation only knowledge of (or an ansatz for) the stimulus space tessellations Ω_r is necessary. In a discrete stimulus ensemble an ansatz for the Ω_r is much simpler to make than for the receptive field vectors \mathbf{w}_r . The distortion measure method has already been applied to analyse SOM models for the development of orientation maps (Riesenhuber *et al* 1997a, b).

3.2. Stimulus overlaps in the ocular dominance model

For the stimuli described in the previous section the overlap $\mathbf{v} \cdot \mathbf{v}'$ is simpler to calculate than the squared difference $(\mathbf{v} - \mathbf{v}')^2$, we will therefore consider the measure

$$E = - \sum_{\mathbf{r}, \mathbf{r}'} h(\Delta \mathbf{r}) w(\mathbf{r}, \mathbf{r}') \quad (6)$$

where

$$w(\mathbf{r}, \mathbf{r}') = \sum_{\mathbf{v} \in \Omega_{\mathbf{r}}, \mathbf{v}' \in \Omega_{\mathbf{r}'}} \mathbf{v} \cdot \mathbf{v}'. \quad (7)$$

Here $\Delta \mathbf{r} = \mathbf{r} - \mathbf{r}'$ denotes the difference in cortical coordinates. The distortion measure in equation (6) equals E_v up to a constant. The factor $w(\mathbf{r}, \mathbf{r}')$ may be interpreted as the interaction energy of the tessellation regions $\Omega_{\mathbf{r}}$ and $\Omega_{\mathbf{r}'}$.

In order to evaluate $w(\mathbf{r}, \mathbf{r}')$ we have to calculate overlaps $\mathbf{v} \cdot \mathbf{v}'$, i.e. between stimuli with centres at \mathbf{x}_0 and \mathbf{x}'_0 . This involves the terms

$$\begin{aligned} \delta^{\text{ll}}(\mathbf{x}_0, \mathbf{x}'_0) &= v^{\mathbf{x}_0, \text{l}} \cdot v^{\mathbf{x}'_0, \text{l}} & \delta^{\text{rr}}(\mathbf{x}_0, \mathbf{x}'_0) &= v^{\mathbf{x}_0, \text{r}} \cdot v^{\mathbf{x}'_0, \text{r}} \\ \delta^{\text{lr}}(\mathbf{x}_0, \mathbf{x}'_0) &= v^{\mathbf{x}_0, \text{l}} \cdot v^{\mathbf{x}'_0, \text{r}} & \delta^{\text{rl}}(\mathbf{x}_0, \mathbf{x}'_0) &= v^{\mathbf{x}_0, \text{r}} \cdot v^{\mathbf{x}'_0, \text{l}} \end{aligned} \quad (8)$$

where $v^{\mathbf{x}_0, \text{l}}$ denotes the component of the stimulus vector \mathbf{v} at retinal position \mathbf{x}_0 in the left eye, and $v^{\mathbf{x}_0, \text{r}}$ denotes that in the right eye. Due to symmetry properties of the system the overlaps in (8) can be expressed in terms of a single function $\delta(\Delta \mathbf{x}_0)$, which explicitly depends on the distance between stimuli peaks, $\Delta \mathbf{x}_0 = \mathbf{x}'_0 - \mathbf{x}_0$:

$$\begin{aligned} \delta^{\text{ll}}(\mathbf{x}_0, \mathbf{x}'_0) &= \delta^{\text{rr}}(\mathbf{x}_0, \mathbf{x}'_0) = \delta(\Delta \mathbf{x}_0) \\ \delta^{\text{lr}}(\mathbf{x}_0, \mathbf{x}'_0) &= \delta^{\text{rl}}(\mathbf{x}_0, \mathbf{x}'_0) = \frac{2c}{1+c^2} \delta(\Delta \mathbf{x}_0) \end{aligned}$$

where

$$\delta(\Delta \mathbf{x}_0) = (1+c^2) \sqrt{\pi \sigma_s^2} \exp\left(-\frac{\Delta \mathbf{x}_0^2}{4\sigma_s^2}\right). \quad (9)$$

3.3. Stimulus space tessellations in the ocular dominance model

As the next step in our analysis, we have to make an ansatz for potentially stationary tessellations $\{\Omega_r\}_{r \in C}$, i.e. for ways the stimuli are distributed among the cortical units. This ansatz is the central part of the analysis, and will be explained in a rather detailed fashion.

To simplify the analysis, we assume in the following that stimuli can only be centred at the locations of the retinal channels. This leaves us with twice as many stimuli as cortical units. Two sensible further assumptions about the tessellation are:

- Due to symmetry each Ω_r contains an equal number of stimuli, i.e. two stimuli.
- Each Ω_r is connected, e.g. the stimuli it contains are neighbours in stimulus parameter space.

These two assumptions allow only three types of tessellation regions in the stimulus parameter space which are depicted in figure 2. In this figure stimulus parameter space is represented as a three-dimensional box, consisting of the discrete two-dimensional retinal coordinates of the stimuli and their ocular bias (L and R denoting whether the larger peak occurs in the left or right retina). The Voronoi polygons $\{\Omega_r\}_{r \in C}$ are subsets of the stimulus parameter space and tessellate it. Type \mathcal{A} is a tessellation region Ω_r which consists of a left eye and a right eye stimulus centred at the same retinal position \mathbf{x}_0 . The corresponding cortical cell at \mathbf{r} is binocular, responding to stimuli in the left and right eye equally well. The simplest tessellation of the entire stimulus parameter space employing this type of Voronoi polygon is shown in the top part of figure 2.

Type \mathcal{B} and \mathcal{C} Voronoi polygons also respect the assumptions on Ω_r previously made. Here, two complementary Voronoi polygons consist of two stimuli which are centred at neighbouring retinal locations. When both stimuli in Ω_r are of the same ocularity,

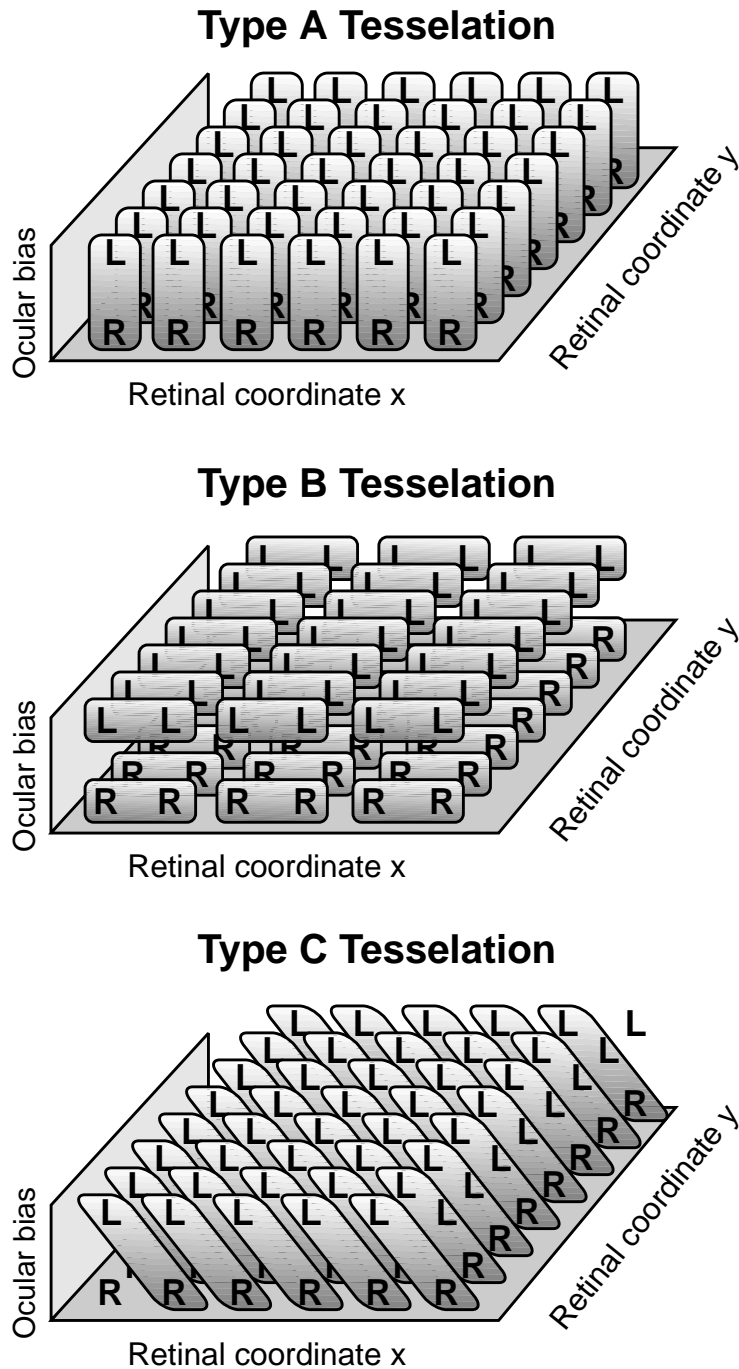


Figure 2. The assumptions of two neighbouring stimuli per Voronoi polygon allow only three types of stimulus space tessellations Ω_r . *Top:* Type *A*, stimuli of different ocularity, but centered at the same retinal location in one Ω_r . *Center:* Type *B*, stimuli of the same ocularity but centered at neighbouring retinal location in one Ω_r . *Bottom:* Type *C*, stimuli of different ocularity at neighbouring retinal locations in one Ω_r . L and R denote the ocular bias of the stimuli (i.e. a larger peak in the left or right retina).

monocularly responding cortical neurons result (type \mathcal{B}). When they are of opposite ocularity, binocular neurons with displaced receptive field centres for the two eyes result (type \mathcal{C}). Possible type \mathcal{B} and \mathcal{C} tessellations of stimulus parameter space is shown in the middle and bottom of figure 2, respectively.

These three types of Ω_r correspond to different receptive field properties of individual neurons. Note that in figure 2 we have not yet equipped the set of Voronoi polygons $\{\Omega_r\}_{r \in \mathcal{C}}$ with neighbourhood properties resulting from the topography of the set of cortical units $r \in \mathcal{C}$. To make the tessellation ansatz complete, by assigning a specific Ω_r to each cortical neuron, we also have to make assumptions about different map layouts, i.e. about the way the Ω_r differ for neighbouring neurons. Here, we distinguish four different kinds of map layouts:

- Binocular state with type \mathcal{A} tessellation.
- Ocular dominance bands of width b , type \mathcal{B} tessellation.
- Ocular dominance of infinite bandwidth, type \mathcal{B} tessellation.
- Binocular state with type \mathcal{C} tessellation.

These map layouts will be dealt with separately in the following subsections. Other kinds of layouts were tested for the sake of completeness, but none turned out to be of interest (e.g. none leads to a lowest energy state).

3.3.1. Binocular state with type \mathcal{A} tessellation. In the rather trivial state of the map which exhibits no ocular dominance each neuron has a tessellation region of type \mathcal{A} , and the Ω_r of neighbouring neurons in the cortex contain stimuli neighbouring in retinal space (figure 3, top). The connected beads in the figure represent the topography of the cortical response unit. These are superimposed on the Voronoi polygons in stimulus parameter space they belong to. For clarity, only one retinal coordinate (x) is displayed in the figure. The topography along the other retinal coordinate (y) is retinotopic in all cases; that is, neighbouring Voronoi polygons in stimulus parameter space belong to neighbouring cortical response units.

In order to finally evaluate E for this or any other tessellation, we must specify the factor $w(\mathbf{r}, \mathbf{r}')$ occurring in equation (6). While $w(\mathbf{r}, \mathbf{r}')$ explicitly depends on the cortical neurons \mathbf{r}, \mathbf{r}' , it depends via the map layout ansatz on the retinal distance $\Delta \mathbf{x} = \mathbf{x}' - \mathbf{x}$ between the centres \mathbf{x}' and \mathbf{x} of the tessellation region Ω_r and $\Omega_{r'}$,

$$w(\mathbf{r}, \mathbf{r}') = w(\Delta \mathbf{x}(\mathbf{r}, \mathbf{r}')).$$

For the present tessellation with regions of type \mathcal{A} we have

$$w(\Delta \mathbf{x}) = 2 \frac{(1+c)^2}{1+c^2} \delta(\Delta \mathbf{x})$$

where $\delta(\Delta \mathbf{x})$ is taken from (9). Since the present tessellation is retinotopic, we further have

$$\begin{aligned} \Delta \mathbf{x} &= \Delta \mathbf{r} \\ w(\Delta \mathbf{x}(\mathbf{r}, \mathbf{r}')) &= w(\Delta \mathbf{x}(\Delta \mathbf{r})) = w(\Delta \mathbf{r}) \end{aligned}$$

yielding the final expression for the distortion measure

$$E^0 = -2 \frac{(1+c)^2}{1+c^2} \sum_{\mathbf{r}, \mathbf{r}'} h(\Delta \mathbf{r}) \delta(\Delta \mathbf{r}). \quad (10)$$

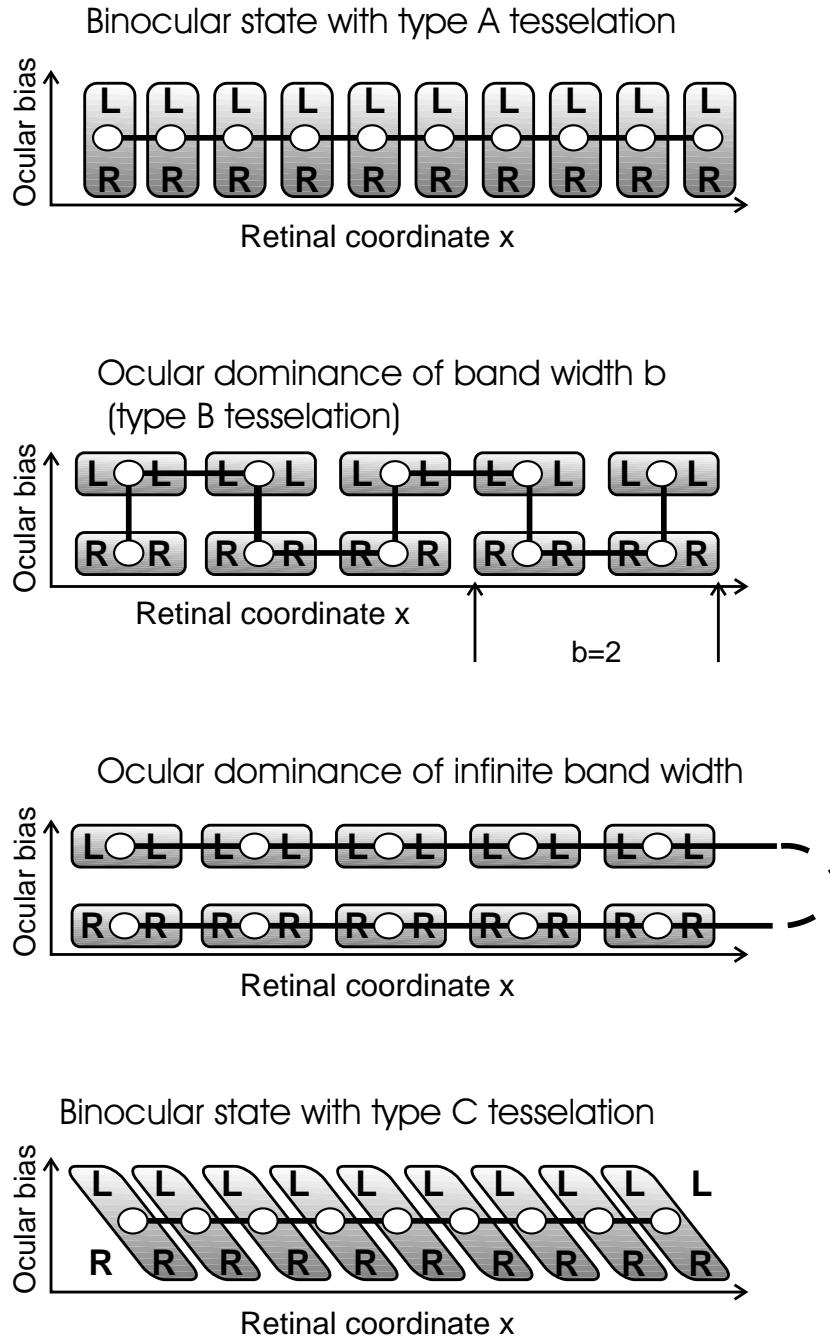


Figure 3. Different possible map layouts for ocular dominance maps (only one retinal coordinate (x) is shown; the maps are organized retinotopically along the other retinal coordinate (y)). *Top:* Type A tessellation regions are retinotopically distributed among map neurons, resulting in a binocular state. *Second from top:* Type B tessellation regions are distributed among map neurons such that bands of width b result, in this case $b = 2$. *Second from bottom:* Type B tessellation regions with infinite bandwidth. *Bottom:* Type C tessellation regions are distributed retinotopically, resulting in a binocular map state.

3.3.2. *Ocular dominance bands of width b , type \mathcal{B} tessellation.* Next we consider a map layout with ocular dominance bands of width b . Here, the Voronoi cells have a spatial extension. Without loss of generality we assume this extension to be in the x -direction (see figure 2). The neighbourhood relations between the neurons corresponding to these cells is such that along the x -direction b left-eye neurons alternate with b right-eye neurons, then another b left-eye neurons, etc (figure 3). In the y -direction, ocularity does not change. So the ‘folding’ of ocularity can be said to run parallel to the extension of the Voronoi cells. We also investigated the orthogonal case (Voronoi cells extended in x -direction, alternating bands in y -direction). This, however, always leads to a higher value of the distortion measure and will not be considered any further.

So in the presently discussed state the symmetry between both coordinates of the layers is broken, and we have to treat the dependence on each coordinate separately in the functions of concern:

$$\begin{aligned} \mathbf{r} &= (r_1, r_2)^t & \mathbf{x} &= (x_1, x_2)^t \\ h(\mathbf{r}) &= h(r_1, r_2) & \delta(\mathbf{x}) &= \delta(x_1, x_2). \end{aligned}$$

Since we have left eye bias and right eye bias tessellation regions here, there are different types of interactions between them, namely w^{ll} , w^{rr} , w^{lr} , and w^{rl} . Due to the symmetry properties of the stimuli, the interaction terms can all be expressed in terms of a single function $D(x_1, x_2)$:

$$\begin{aligned} w^{\text{ll}}(x_1, x_2) &= w^{\text{rr}}(x_1, x_2) = D(x_1, x_2) \\ w^{\text{lr}}(x_1, x_2) &= w^{\text{rl}}(x_1, x_2) = \frac{2c}{1+c^2} D(x_1, x_2) \\ D(x_1, x_2) &= 2\delta(x_1, x_2) + \delta(x_1 + 1, x_2) + \delta(x_1 - 1, x_2). \end{aligned} \quad (11)$$

To evaluate E it is more convenient to rewrite equation (6) as a sum of interaction terms $\delta_{ss'}$ between stripes, where $s, s' = 0, \pm 1, \pm 2, \dots$, denotes the index of a stripe,

$$\begin{aligned} E^b &= - \sum_{s, s'} \Gamma(\Delta s) \delta_{ss'} \\ \Gamma(\Delta s) &= \begin{cases} 1 & \text{if } \Delta s \text{ even} \\ \frac{2c}{1+c^2} & \text{if } \Delta s \text{ odd} \end{cases} \\ \delta_{ss'} &= \sum_{r_2, r_2'} \sum_{i, i'=0}^{b-1} h(b\Delta s + \Delta i, \Delta r_2) D(\Delta x_1, \Delta x_2). \end{aligned} \quad (12)$$

$\Delta s = s - s'$ denotes the difference in stripe indices. The factor $\Gamma(\Delta s)$ takes into account the difference in interactions between stripes of equal ocularity and interactions of stripes with opposite ocularity. In each term $\delta_{ss'}$ the interactions between the receptive fields contained in the stripes s and s' are traced (i and i' are the internal coordinates of tessellation regions in s and s' respectively, $\Delta i = i' - i$; note that r_2 runs along the bands, r_1 runs perpendicular to the bands).

The retinal distances in the system are now

$$\Delta x_1 = b\Delta s + 2\Delta i \quad \Delta x_2 = \Delta r_2.$$

The latter expressions inserted into equation (12) yield the final result for the distortion measure in ocular dominance solutions:

$$E^b = - \sum_{r_2, r_2'} \sum_{s, s'} \sum_{i, i'=0}^{b-1} \Gamma(\Delta s) h(b\Delta s + \Delta i, \Delta r_2) D(b\Delta s + 2\Delta i, \Delta r_2). \quad (13)$$

3.3.3. *Ocular dominance of infinite bandwidth, type B tessellation.* Figure 3 depicts an infinite bandwidth solution, with type B tessellation regions arranged such that neighbouring neurons have identical ocularity. The interaction term between different receptive fields is $D(x_1, x_2)$ as given in equation (11). However, there is a difference in the retinal distances

$$\Delta x_1 = 2\Delta r_1 \quad \text{and} \quad \Delta x_2 = \Delta r_2$$

which yields the final result

$$E^\infty = - \sum_{r_1, r_1'} \sum_{r_2, r_2'} h(\Delta r_1, \Delta r_2) D(2\Delta r_1, \Delta r_2). \quad (14)$$

3.3.4. *Binocular state with type C tessellation.* Finally we consider the tessellation with binocular cells, but on the basis of type C tessellation regions (figure 3 (bottom)). This state is retinotopic, as the binocular state discussed above. The difference lies in the structure of the tessellation regions which are now of type C instead of type A. For this state we can obtain an expression for the distortion measure E^c in a similar manner as in the above cases:

$$E^c = - \sum_{r_1, r_1'} \sum_{r_2, r_2'} h(\Delta r_1, \Delta r_2) w(\Delta r_1, \Delta r_2) \quad (15)$$

$$w(r_1, r_2) = 2\delta(r_1, r_2) + \frac{2c}{1+c^2} (\delta(r_1+1, r_2) + \delta(r_1-1, r_2)).$$

Comparing this distortion energy to that of the binocular state with type A tessellation, one can show that $E^c > E^0$ for all values of the relevant parameters. A state with type C tessellations therefore is never attained, and we can disregard this state in the following.

3.4. Analytical phase diagrams

In the final step of the analysis we now determine the lowest energy state for a particular combination of parameters. This is done by numerically performing the summation in equations (10), (13), (14) and (15). By varying the control parameters of the system, the width σ of the SOM lateral interaction function and the stimulus correlation parameter c , we can obtain phase diagrams of the system which indicate the parameter regimes for each of the states.

Two such phase diagrams, for a width $\sigma_s = 2.0$ and $\sigma_s = 4.0$ of the stimuli, are shown in figure 4. Among the possible ocular dominance states, we considered states with a bandwidth from $b = 1$ up to $b = 6$ (note that a bandwidth of $b = 1$ corresponds to a wavelength of $\lambda = 2$ of the pattern), and the state with infinite bandwidth. Solid phase transition lines separate regions in which different states prevail. The dotted phase transition lines indicate the structure of the phase diagram when the state with infinite bandwidth is not considered in the computation.

Consider the phase diagram on the left of the figure ($\sigma_s = 2.0$). Above a value of $c \approx 0.6$, binocularity occurs, depicted by the grey square. Below a critical value of c , which decreases slightly with increasing σ , ocular dominance states occur. Among these, states with lower width occur at larger values of c . This dependence of the bandwidth on the correlation parameter is particularly apparent, if the infinite bandwidth state is not considered. However, even if this state is included in the comparison, a parameter regime exists in which this unphysiological state does not occur (see the discussion in section 5).

The differences in distortion between the binocular state and the various ocular dominance states are substantial compared with the changes of E as a function of c . So,

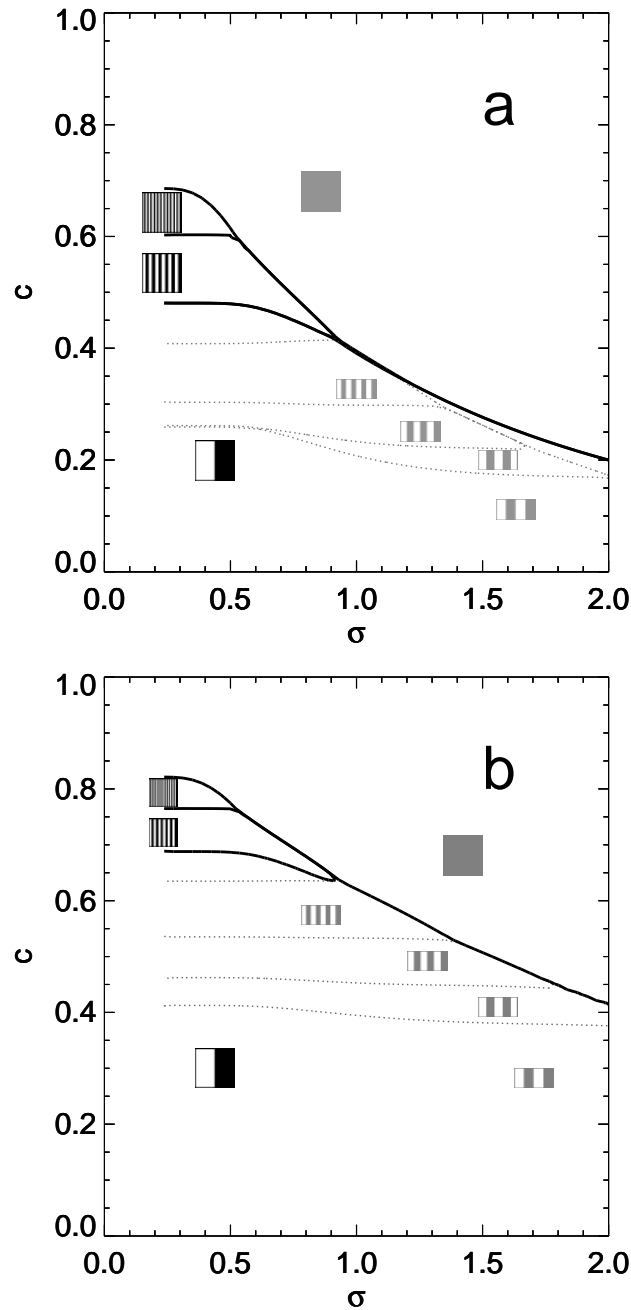


Figure 4. Two phase diagrams for an SOM model for the development of ocular dominance maps for stimulus widths (a) $\sigma_s = 2$ and (b) $\sigma_s = 4$. Parameters c and σ denote the amount of correlation between eyes, and the width of the map neighbourhood function, respectively. If the infinite bandwidth state is taken into account, only four different states occur (binocular state \mathcal{A} , monocular states with bandwidths $b = 1$, $b = 2$, and $b = \infty$). These states are indicated by the square-shaped icons, and are separated by the solid lines. If the infinite bandwidth state is not taken into account, monocular states with an increasing bandwidth occur in the phase diagram (indicated by the rectangular icons, separated by the dotted lines).

the results for the critical c for the transition from binocularity to ocular dominance can be regarded as an analytical prediction of an explicit state transition from one state to another. In contrast, the differences between the E values for the different ocular dominance states are rather small. Considering the rather crude assumptions made with respect to the map layout, one should neither expect the assumed states nor transitions between them to materialize explicitly in a simulation. Instead, one should interpret the phase diagram within the ocular dominance regime as showing a broadening of ocular dominance bands with decreasing between-eye correlation c . Such an effect has recently been observed in an experiment in the cat (Löwel 1994); it may turn out to be crucial in comparison of explanatory power of different map formation models (see the discussion in section 5).

The comparatively small distortion differences between the ocular dominance states also mean that as far as the main transition from binocularity to ocular dominance is concerned, the assumptions made for the ocular dominance map layout are not crucial.

The results depicted in figure 4 were generated for a stimulus width $\sigma_s = 2.0$ and $\sigma_s = 4.0$. Note that the qualitative features of the phase diagrams remain the same; the overall structure of the phase diagrams is not altered by variations of the stimulus width (we also checked $\sigma_s = 0.5, 1$).

4. Numerical results

4.1. Comparison of analytical and numerical energy values

In order to complement our analytical results by numerical evidence, we performed several simulations of ocular dominance formation in this model. In a first series of simulations we specifically addressed the question, to what extent numerically and/or analytically determined values for E_w and E_v coincide. We simulated maps at various values of the correlation parameter c using the reduced stimulus set employed in the mathematical analysis (stimuli with central peak in either eye, centred at each retinal channel, respectively). We then computed the average degree of ocularity

$$O = \langle \|\mathbf{w}_{r, \text{left eye}} - \mathbf{w}_{r, \text{right eye}}\| \rangle_r.$$

This measure (shown as a solid line in figure 5 (left)) indicates a state transition at $c = 0.66$. We further determined numerical values of E_w and E_v by evaluating equations (4) and (5) for the reduced stimulus set. The close resemblance of the two interpolated lines $E_w(c)$ (crosses) and $E_v(c)$ (stars) demonstrates that the error made in replacing E_w by the much simpler evaluable E_v is not significant.

The analytical values for E_v for the two map states are depicted in figure 5 (right) as a dashed line (binocularity) and a dotted line (ocular dominance). The crossover between the two lines at $c = 0.68$ coincides very closely with the numerically observed transition at $c \approx 0.66$.

The numerically determined values for E_v come very close to the analytical values for the respective type of solution ($E_{v, \text{OD}}$ at $c < 0.66$, $E_{v, \text{non-OD}}$ at $c > 0.66$). Note here that the simulations allow only the determination of E_v for that state of the map which is actually attained by the map formation algorithm; hypothetical other states are not accessible.

The inset in the left part of figure 5 supplements the analytical results depicted in figure 4. It shows that $E_v(c)$ for the binocular state (dashed line) takes a substantially different course than $E_v(c)$ for the ocular dominance solution, while the $E_v(c)$ for the different ocular dominance solutions (stripe width 1, 2, or $N/2$) remain rather close to each

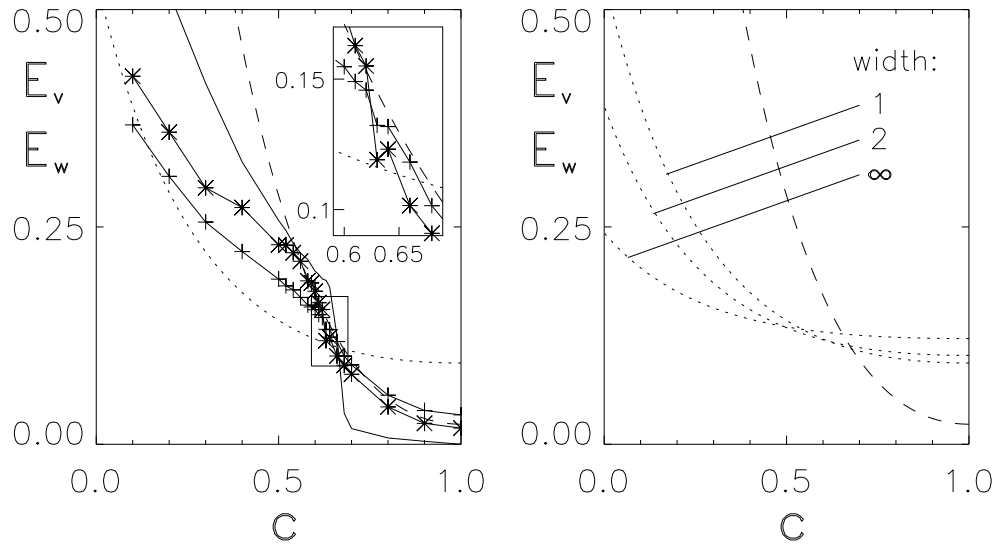


Figure 5. Distortions E_v and E_w as a function of stimulus correlations c for the SOM ocular dominance model. *Left:* Dashed line: analytical E_v of non-OD solution; dotted line: analytical E_v of OD solution (width 1); solid line: mean ocularity $O = \langle \|\mathbf{w}_{r, \text{left eye}} - \mathbf{w}_{r, \text{right eye}}\| \rangle_r$, indicating a state transition at $c = 0.66$; solid line with stars: numerical E_v ; solid line with crosses: numerical E_w . The E_v values were scaled in order to compensate for the additional summation as compared to E_w . The inset is an enlargement of the cross-over region. *Right:* Analytical E_v of binocular solution (dashed line), together with three analytical E_v of ocular dominance solutions with increasing width. Note that for decreasing c , the minimal value for E_v is attained for solutions with increasing bandwidth.

other. As pointed out in the previous section, this observation means that the transition point for the occurrence of ocular dominance does not depend much on the layout assumed for the ocular dominance map.

4.2. Numerical phase diagrams

In a next step, we went back to the full stimulus set and simulated maps at various values of σ , c and σ_s , using stimuli centred at any location. The critical values c_{crit} for ocular dominance to occur are shown in figure 6 for two typical widths σ_s of the stimuli, together with the analytical solution (solid line). The agreement between calculated and simulated values is remarkably good, considering the crude approximations made during the analysis.

4.3. Multiplicative versus subtractive normalization

Finally we addressed a specific point of the simulation procedure, the normalization scheme. In the present map formation model, as well as in most other developmental models, the values of synaptic weights are increased according to a Hebbian rule (the $\epsilon h_{rs} v$ part of the learning rule (1)). To prohibit an unlimited growth of synaptic weights, a normalization of the weights has to be performed. In the present model, the normalization is done in a multiplicative fashion, with the term normalizing a weight vector \mathbf{w}_r being proportional to the weight vector itself (the $-\epsilon h_{rs} \mathbf{w}_r$ part of the learning rule, equation (1)). An alternative

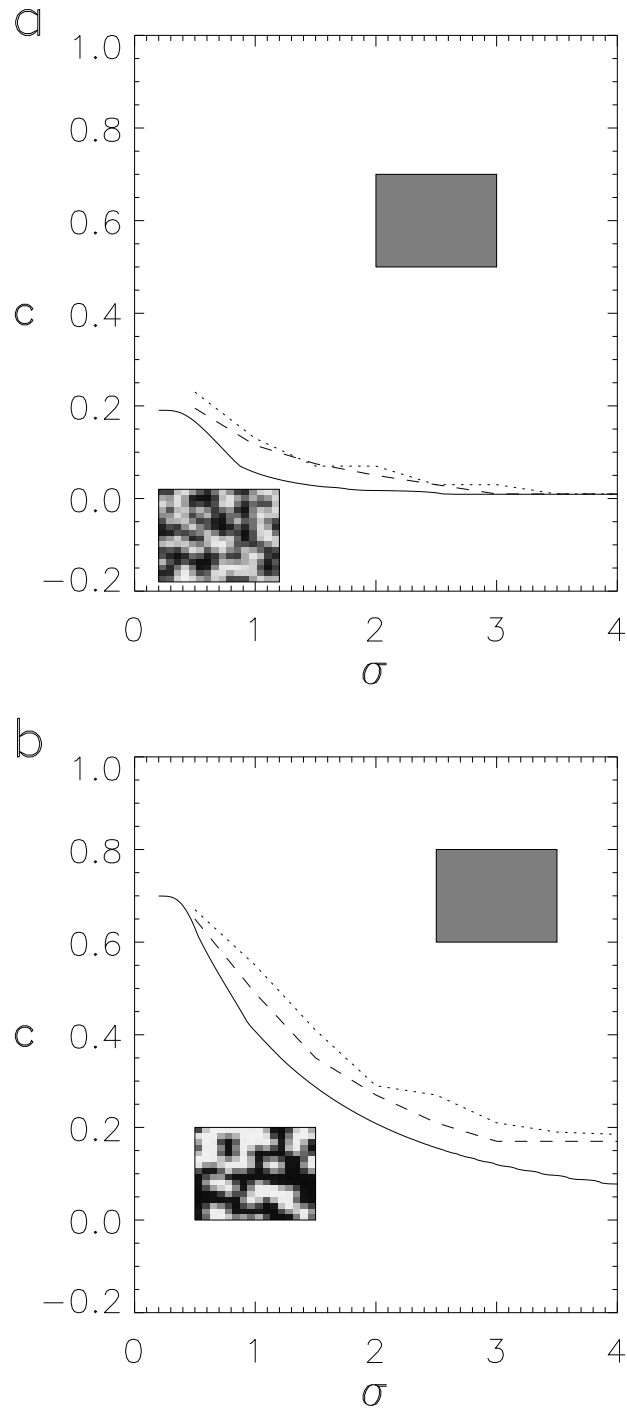


Figure 6. Comparison of numerical and analytical results for the transition from binocularity (above curves) to ocular dominance (below curves, see exemplary inset maps), for stimulus widths (a) $\sigma_s = 0.5$ and (b) $\sigma_s = 2.0$. Solid lines: analytical; dashed lines: multiplicative normalization; dotted lines: subtractive normalization.

normalization scheme, subtractive normalization, diminishes a weight vector by a constant amount for each channel, followed by a rectification step, and a multiplicative normalization to fine tune for deviations of the norm of the weight vector due to the rectification. It has been pointed out (Miller and MacKay 1994, Goodhill 1994) that these different normalization schemes can have an impact on the developmental dynamics. Consequently, they could have an influence on the structure emerging.

The analysis technique applied in this paper evaluates only final states of an SOM. An underlying assumption is that the detailed course of the developmental dynamics can be neglected as long as the final state, the minimum energy state, is attained. Therefore, it is an interesting test to see if the locations of the state transitions observed in this model depend on the normalization procedure or not. In a final series of simulations we investigated a variant of the SOMs, where a subtractive normalization is implemented in the following way:

$$\mathbf{w}_r(t+1) = \frac{\left[\mathbf{w}_r(t) + \epsilon h(\mathbf{r} - \mathbf{s})\mathbf{v} - \epsilon h(\mathbf{r} - \mathbf{s}) \frac{\mathbf{1}}{\|\mathbf{1}\|} \right]_+}{\left\| \left[\mathbf{w}_r(t) + \epsilon h(\mathbf{r} - \mathbf{s})\mathbf{v} - \epsilon h(\mathbf{r} - \mathbf{s}) \frac{\mathbf{1}}{\|\mathbf{1}\|} \right]_+ \right\|}. \quad (16)$$

Here, $[\cdot]_+$ means rectification, and $\|\cdot\|$ denotes a sum norm. So normalization was achieved by subtraction of a constant uniform sum-normalized vector, followed by rectification, and subsequent divisive normalization to fine tune for possible changes of the normalization due to the rectification process.

The results for the phase transitions are plotted in figure 6 as dashed curves for multiplicative normalization and dotted curves for subtractive normalization. The results for both normalizations agree quite well with the analytical result (solid curves). The deviations between subtractive and multiplicative normalization are smaller than the deviation of either one to the analytical solution, such that the assumption, on which our analysis is based, of independence from the details of the developmental dynamics seems to hold.

5. Discussion

In this paper, we have analytically solved a high-dimensional SOM-based model for the development of ocular dominance maps. The analysis is based on the evaluation of a distortion measure for different possible final states of the map. The distortion measure involves sums over the sets of stimuli Ω_r which map to particular neurons r . To facilitate the evaluation of these sums, we considered in the analysis only a minimal set of stimuli, i.e. two stimuli per neuron. With this simplified stimulus set, the binocular and ocular dominance states can be characterized as mapping stimuli from either eye, but located at the same retinal position to one neuron, or mapping stimuli from neighbouring retinal positions, but from the same eye to one neuron. The error introduced by this reduction of the number of stimuli is small, as evidenced by our numerical tests which corroborate the analytically calculated critical values for the correlation parameter c quite well.

Our analysis mathematically underlines two pattern-formation properties of this ocular dominance model which make the model attractive from a neurobiological point of view. Ocular dominance solutions can occur here even at positive correlations between eyes ($c > 0$). Judging from the four different sets of stimuli we investigated, this property does not depend on the stimulus size. In contrast, a perturbation analysis of correlation-based models (Dayan and Goodhill 1992) showed a tendency towards binocularity even for only small positive between-eye correlations. Furthermore, the length scale of the emerging

patterns, i.e. the width of the ocular dominance bands, does increase with a decreasing correlation parameter c . This property of the model, which was in fact provided in advance on numerical grounds in Goodhill (1993), nicely matches a recent neuroanatomical observation by Löwel (1994), where strabismic cats (interpreted here as having smaller between-eye correlations) were shown to exhibit broader ocular dominance bands than normal-sighted cats.

In our analysis we considered, among the different ocular dominance states, one state with infinite bandwidth. This amounts to two spatially separate retinotopic representations for the two eyes within one cortical area—a clearly unphysiological state. This state in principal can occur in many models, and has been noted to minimize energy functions (Dayan 1993). It is an interesting aspect of our analysis that there are regimes in parameter space where this state is not the energetically optimal one. While other arguments to dismiss the existence of this state (in particular the argument that retinotopy is established before ocular dominance and cannot be refined to such a large degree, see von der Malsburg (1994)) remain fully valid, we here have the additional argument that even from a map energy point of view this state need not dominate.

The present analysis rests on an evaluation of the final state of the map, without explicit consideration of the dynamics which lead to this state (apart from the assumption that the dynamics do indeed lead to the energetically optimal state). A competing method of analysis for SOMs considers the stability of particular states under the learning dynamics (Ritter *et al* 1992, Obermayer *et al* 1992). This latter approach has been applied to the feature map variant of the SOM, where receptive fields are described by a small number of parameters. In contrast, our distortion measure method is specifically suited for high-dimensional SOMs, where receptive fields are explicitly modelled as synaptic weight vectors with internal structure. The stability analysis method for feature space SOMs enables the wavelength of unstable modes of the map to be calculated. The dependence of the wavelength on the SOM neighbourhood width σ , on a possible decrease ('cooling') of σ during development, and on parameters related to the correlation between eyes, is intricate and requires detailed discussion (see Pawelzik *et al* 1995, Scherf *et al* 1996).

In order to test whether or not our results are indeed independent of the details of the developmental dynamics, we also simulated maps with a subtractive normalization procedure, a variation of the multiplicative normalization usually employed for SOMs. The close match of numerical results for either normalization procedure is interesting in its own right. In recent years, various investigations (Miller and MacKay 1994, Goodhill and Barrow 1994) have focused on the consequences of different normalization procedures in map-formation algorithms. While these authors found, in their map-formation models and examples, that the subtractive normalization leads to more 'sharpened' receptive fields, representing 'extreme' inputs, these results apply in a strict sense only to the particular models and/or stimulus set employed in these investigations. We report here that in the present SOM model both normalization schemes lead to identical results for the transition to non-trivial patterns. This discrepancy may arise from the strong nonlinearity employed in the SOM-mapping rule as opposed to the linear Hebbian learning employed by Miller and MacKay (1994). The difference between multiplicative and subtractive normalization could be larger if stimuli of an extension substantially larger than a receptive field size are used. This hypothetical consequence of very large stimuli could be the explanation of the failure to find ocular dominance maps with multiplicative normalization in competitive Hebbian models, as reported by Goodhill (1993) and Goodhill and Barrow (1994). Our results rather suggest that the difference between the normalization schemes might be case-dependent and might play a less prominent role than previously anticipated.

Acknowledgments

This work has been supported by the Deutsche Forschungsgemeinschaft through SFB 185 'Nichtlineare Dynamik', TP E6.

References

- Bauer H-U 1995 Development of oriented ocular dominance bands as a consequence of areal geometry *Neural Comput.* **7** 36–50
- Bauer H-U, Riesenhuber M and Geisel T 1996 Phase diagrams of self-organizing maps *Phys. Rev. E* **54** 2807–10
- Dayan P 1993 Arbitrary elastic topologies and ocular dominance *Neural Comput.* **5** 392–401
- Dayan P and Goodhill G 1992 Perturbing Hebbian rules *Advances in Neural Information Processing Systems 4* ed J E Moody *et al* (San Mateo, CA: Morgan Kaufman) pp 19–26
- Durbin R and Mitchison G 1990 A dimension-reducing framework for cortical maps *Nature* **343** 644–7
- Erwin E, Obermayer K and Schulten K 1995 Models of orientation and ocular dominance columns in visual cortex *Neural Comput.* **7** 425–68
- Goodhill G J 1993 Topography and ocular dominance: a model exploring positive correlations *Biol. Cybern.* **69** 109–18
- Goodhill G J and Barrow H G 1994 The role of weight normalization in competitive learning *Neural Comput.* **6** 225–70
- Goodhill G J and Willshaw D J 1990 Application of the elastic net algorithm to the formation of ocular dominance stripes *Network: Comput. Neural Syst.* **1** 41–59
- Kohonen T 1982 Self-organized formation of topologically correct feature maps *Biol. Cybern.* **43** 59
- 1995 *The Self-Organizing Map* (Berlin: Springer)
- Löwel S 1994 Ocular dominance column development: strabismus changes the spacing of adjacent columns in cat visual cortex *J. Neurosci.* **14** 7451–68
- Miller K D, Keller J B and Stryker M P 1989 Ocular dominance column development: analysis and simulation *Science* **245** 605–15
- Miller K D 1994 A model for the development of simple-cell receptive fields and the ordered arrangement of orientation columns through activity dependent competition between on- and off-center inputs *J. Neurosci.* **14** 409–41
- Miller K D and MacKay D J C 1994 The role of constraints in Hebbian learning *Neural Comput.* **6** 100–26
- Mitchison G 1995 A type of duality between self-organizing maps and minimal wiring *Neural Comput.* **7** 25–35
- Obermayer K, Blasdel G G and Schulten K 1992 Statistical-mechanical analysis of self-organization and pattern formation during the development of visual maps *Phys. Rev. A* **45** 7568–89
- Obermayer K, Ritter H and Schulten K 1990 A principle for the formation of the spatial structure of cortical feature maps *Proc. Natl Acad. Sci.* **87** 8345–9
- Pawelzik K, Scherf O, Wolf F and Geisel T 1995 Correlation dependence of ocular dominance patterns requires receptive field shrinkage during development *Computational Neuroscience, Trends in Research* ed J M Bower (New York: Academic) pp 239–44
- Riesenhuber M, Bauer H-U and Geisel T 1997a Analyzing phase transitions in high-dimensional self-organizing maps *Biol. Cybern.* at press
- 1997b On-center and off-center cell competition generates oriented receptive fields from non-oriented stimuli in Kohonen's self-organizing map *Proc. Computational Neuroscience (CNS) 1996 (Boston, MA)* ed J M Bower (New York: Plenum) at press
- Ritter H, Martinetz T and Schulten K 1992 *Neural Computation and Self-Organizing Maps* (Reading, MA: Addison-Wesley)
- Scherf O, Pawelzik K, Wolf F and Geisel T 1996 in preparation
- Swindale N V 1980 A model for the formation of ocular dominance stripes *Proc. R. Soc.* **208** 243–64
- 1996 The development of topography in the visual cortex: a review of models *Network: Comput. Neural Syst.* **7** 161–247
- Tanaka S 1990 Theory of self-organization of cortical maps: mathematical framework *Neural Networks* **3** 625–40
- von der Malsburg C 1973 Self-organization of orientation sensitive cells in the striate cortex *Kybernetik* **14** 81–100
- 1979 Development of ocularity domains and growth behaviour of axon terminals *Biol. Cybern.* **32** 49–62
- 1994 Network self-organization in the ontogenesis of the mammalian visual system *Neural and Electronic Networks* ed S F Zornetzer *et al* (New York: Academic)
- Willshaw D J and von der Malsburg C 1976 How patterned neural connections can be set up by self-organization *Proc. R. Soc.* **194** 431–45